Calving controlled by melt-undercutting: detailed calving styles revealed through time-lapse observations

Penelope How,[1,2*] Kristin M. Schild,[3,4] Douglas I. Benn,[5] Riko Noormets,[2] Nina Kirchner,[6] Adrian Luckman,[7,8] Dorothée Vallot,[9] Nicholas R. J. Hulton[1,2] and Chris Borstad[8]

[1]*Institute of Geography, School of GeoSciences, University of Edinburgh, Edinburgh, UK*

[2]*Department of Arctic Geology, University Centre in Svalbard, Longyearbyen, Norway*

[3]*Department of Earth Sciences, University of Oregon, Eugene, USA*

[4]*Climate Change Institute, University of Maine, Orono, USA*

[5]*Department of Geography and Sustainable Development, University of St. Andrews, Fife, UK*

[6]*Department of Physical Geography, Stockholm University, Stockholm, Sweden*

[7]*Department of Geography, College of Science, Swansea University, Swansea, UK*

[8]*Department of Arctic Geophysics, University Centre in Svalbard, Longyearbyen, Norway*

[9]*Department of Earth Sciences, Uppsala University, Uppsala, Sweden*

Correspondence: Penelope How <p.how@york.ac.uk>

ABSTRACT. Here, we present a highly detailed study of calving dynamics at Tunabreen, a tidewater glacier in Svalbard. A time-lapse camera was trained on the terminus and programmed to capture images every three seconds over a 28-hour period in August 2015, producing a highly detailed record of 34,117 images from which 358 individual calving events were distinguished. Calving activity is characterised by frequent events (12.8 events per hour) that are small relative to the spectrum of calving events observed, demonstrating the prevalence of small-scale calving mechanisms. Five calving styles were observed, with a high proportion of calving events (82%) originating at, or above, the waterline. The tidal cycle plays a key role in the timing of calving

events, with 68% occurring on the falling limb of the tide. Calving activity is concentrated where meltwater plumes surface at the glacier front, and a ∼5 m undercut at the base of the glacier suggests that meltwater plumes encourage melt-undercutting. We conclude that frontal ablation at Tunabreen may be paced by submarine melt rates, as suggested from similar observations at glaciers in Svalbard and Alaska. Using submarine melt rate to calculate frontal ablation would greatly simplify estimations of tidewater glacier losses in prognostic models.

INTRODUCTION

The loss of ice from the termini of marine-terminating glaciers (i.e. frontal ablation) occurs by both submarine melting and iceberg calving. Calving from tidewater glaciers can occur by a number of mechanisms, including longitudinal stretching, buoyant instability, and undercutting of the front by submarine melt (Van Der Veen, 2002; Benn and others, 2007). Submarine melting can influence calving by undercutting and destabilising the subaerial part of the ice front. Studies on several glaciers indicate that submarine melting is an important process in settings where relatively warm ocean water interacts with glacier fronts, and efficient heat transfer is promoted by buoyant meltwater plumes (Motyka and others, 2003; Bartholomaus and others, 2013; Chauché and others, 2014; Rignot and others, 2015; Slater and others, 2015; Truffer and Motyka, 2016).

Where melt-undercutting is the dominant driver of calving, frontal ablation rates depend on the relationship between two fundamental factors: 1) the temporal and spatial evolution of subaqueous cavities by melting; and 2) the mechanical response of the ice to the evolving geometry and associated stresses (Joughin and others, 2008; Howat and others, 2010). Although important observations have been made about the morphology of undercut cavities (e.g., Rignot and others, 2015), there is a lack of concurrent data on cavity development and calving events. Our understanding of the relationship between undercutting and calving is therefore heavily reliant on modelling at present.

Melting of submerged ice is a function of water temperature and tangential velocity (Holland and others, 2008; Straneo and others, 2010; Jenkins, 2011). The motion of water up or across an ice front can occur

*Present address: Department of Environment and Geography, University of York, York, UK.

as the result of wind-driven, tidal and other currents (e.g., Bartholomaus and others, 2013; Sutherland and others, 2014; Pętlicki and others, 2015; Schild and others, 2018), or convection driven by the ascent of buoyant meltwater (e.g., Schild and others, 2016). Plumes of meltwater rising from subglacial discharge points and plume-driven secondary circulation patterns are considered to play particularly important roles in submarine melting and melt-undercutting (e.g., Cowton and others, 2015; Slater and others, 2017a,b; Schild and others, 2018; Vallot and others, 2018a).

Experiments with the discrete element model HiDEM (Benn and others, 2017; Vallot and others, 2018a) suggest that calving can occur in response to melt-undercutting in two distinct ways: 1) where undercuts are small, low-magnitude calving can occur via localised collapse of the overhang; and 2) where undercuts are large, high-magnitude calving events can remove all of the overhang plus additional ice. In the latter case, fractures form at the ice surface upglacier of the undercut, and propagate downwards as the ice front bends forward and downward. These contrasting responses to undercutting have important implications for long-term calving rates. If undercuts are able to grow large enough to trigger high-magnitude calving events, long-term calving rates will be greater than the submarine melt rate (i.e. the calving multiplier effect proposed by O'Leary and Christoffersen, 2013). On the other hand, if low-magnitude calving events prevent undercuts from becoming large enough to trigger high-magnitude calving, long-term calving rates will simply equal the undercutting rate. This analysis suggests that the relationship between melt-undercutting and calving can be inferred from detailed observations of calving events, especially calving style.

The magnitude, frequency, and style of calving events are intrinsically linked. Calving activity can range from very small ($<10^4$ m^3) and frequent (>100 d^{-1}) events, to larger ($>10^8$ m^3) and infrequent (<1 d^{-1}) occurrences (Åström and others, 2014; Chapuis and Tetzlaff, 2014). Many large, infrequent calving events have been identified using time-lapse photography (e.g., Rosenau and others, 2013; James and others, 2014; Medrzycka and others, 2016). The calving styles associated with smaller, more frequent events are challenging to document because small calved bergs are difficult to distinguish in satellite images and low-temporal time-lapse photography. Under-representation of small-scale calving styles, and their control on long-term frontal ablation, is therefore an inherent problem.

Here, we examine calving dynamics at Tunabreen, a tidewater glacier in Svalbard, where calving activity is known to be low-magnitude and frequent (Köhler and others, 2015; Luckman and others, 2015). A time-lapse camera was installed on a ridge adjacent to the glacier terminus, capturing images every 3 seconds (Fig. 1A). This produced a highly detailed record of calving events over a period of 28 hours during 7th–8th

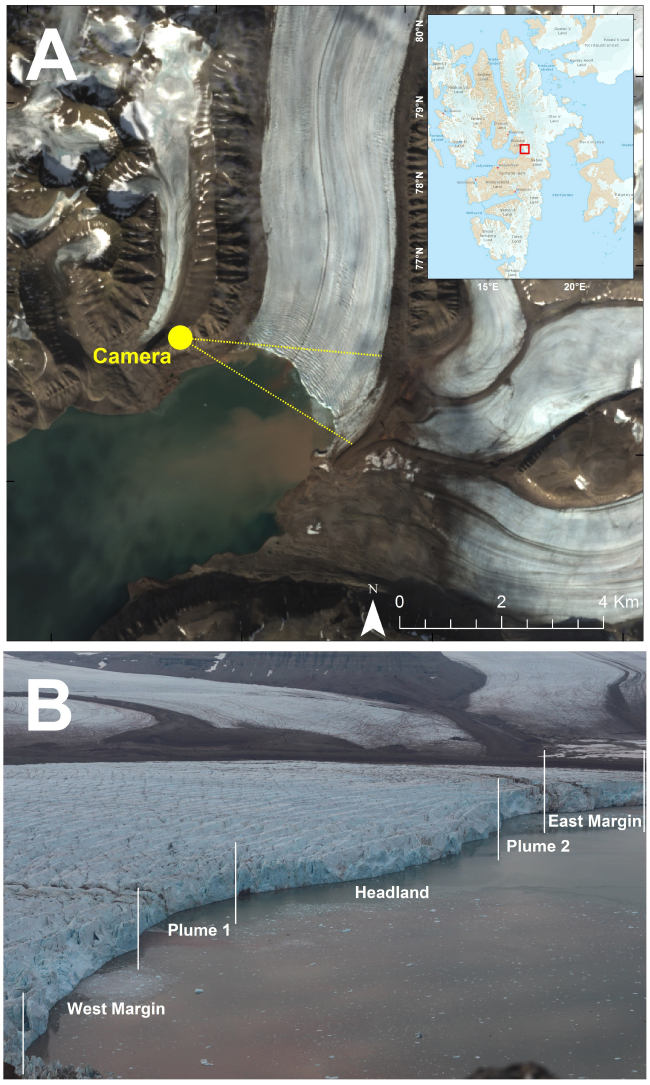

Fig. 1. The lower tongue and calving front of Tunabreen. A) Pan-sharpened Landsat image (17th August 2015), showing the location and viewshed of the time-lapse camera. B) An image from the time-lapse camera, showing the calving front and the partitioned regions of the terminus.

August 2015. Taken together with bathymetric surveys of the sea bed/submarine ice cliff and observations of plume locations, this record allows us to study the processes associated with individual calving events and the role of melt-undercutting.

STUDY AREA

Tunabreen is a marine-terminating, surge-type glacier in Svalbard (78.29°N, 17.25°E, Fig. 1). The glacier terminus is approximately 3 km wide, and calves into Tempelfjorden, a 14 km-long branch of the Isfjorden system. Isfjorden opens into the Atlantic Ocean approximately 90 km west of the glacier, and the circulatory

system of Tempelfjorden is relatively sheltered from the warm West-Spitsbergen Current (WSC) compared to the deeper, unrestricted connection to other fjords such as Kongsfjorden (Cottier and others, 2005; Luckman and others, 2015).

Tunabreen is one of a few glaciers in Svalbard that has been observed to undergo multiple surge cycles, with surge maxima occurring in 1930, 1971, 2004 (Flink and others, 2015), and most recently in 2016 (A. Luckman, pers. comm.). After 2004, the glacier entered a quiescent, slow-flowing phase, with velocities typically between 0.2–1.0 md^{-1} and a maximum frontal ablation rate of $\sim$3.0 md^{-1}. During this quiescent phase (which includes the study period), detectable motion is confined to the lower tongue within $\sim$2 km of the ice front which is related to longitudinal extension in response to the force imbalance at the calving front (Luckman and others, 2015).

The glacier terminates in a relatively shallow part of Tempelfjorden which is 30–50 m deep, and the $\sim$70 m thick ice front is grounded on the sea bed (Flink and others, 2015). Two turbid meltwater plumes surface in the fjord adjacent to the glacier, coinciding with two pronounced embayments in the calving front (noted in Fig. 1B).

Calving activity at Tunabreen has been documented from time-lapse photography (e.g., Åström and others, 2014; Vallot and others, 2018b), passive seismic monitoring (e.g., Köhler and others, 2015), and satellite data (e.g., Luckman and others, 2015). Luckman and others (2015) found a high correlation between ocean temperature and frontal ablation rates, suggesting that melt-undercutting is the dominant control on calving losses on seasonal timescales. However, controls on calving activity at shorter timescales are relatively unexplored.

METHODS

Camera set-up

A time-lapse camera was installed in August 2015 on Ultunafjella, the ridge to the west of the glacier tongue (Fig. 1A). The system consisted of a Canon EOS 700D camera body, an EF 50 mm f/1.8 II fixed focal lens and a Harbortronics Digisnap 2700 intervalometer, which was powered by a 12 V DC battery and a 10 W solar panel. The camera was set to take one photo every three seconds, producing a record that spans a 28-hour period from 19:25 on the 7th August to 23:53 on the 8th August (local time, GMT+2). Images were taken using shutter-priority settings because it was important to capture images across a consistent time window (rather than use aperture-priority settings to achieve consistent light level). Each

Table 1. Calving styles observed at Tunabreen

Style category	Details
Ice-fall event	Small–medium size; typically involves a section of ice breaking off from the subaerial part of the ice front; tend to create a large splash.
Sheet collapse	Medium–large size; ice collapse has little or no rotation, likely to be facilitated by weaknesses at/near the waterline.
Stack topple	Medium–large size; ice collapse rotates outward from ice front indicating an outward force imbalance; failure usually occurs through crevasse propagation.
Waterline event	Small size; small pieces of ice break off at the waterline, normally below or above an undercut section of the ice front; typically generate little noise or splash.
Subaqueous event	Small–large size; ice breaks off from below the waterline and rises to the fjord surface.

image was time-stamped by the clock on the camera. Camera clock drift is a common problem in time-lapse photogrammetry and it is difficult to overcome this limitation without a direct connection to an accurate clock, such as a GPS (Welty and others, 2013). The clock on the camera at Tunabreen drifted by approximately two seconds over the course of the monitoring period, based on the drift in the time stamp. This drift was corrected for in post-processing.

Calving style

In all, 34,117 images were collected, and the style of each calving event was manually determined by examining the time-lapse imagery on a frame-by-frame basis. Each event was noted for the origin of the

Table 2. Calving events observed from the time-lapse image sequence (7th–8th August 2015).

Calving style	Area					Total
	West margin	Plume 1	Headland	Plume 2	East margin	
Ice-fall event	31	30	31	33	30	155
Sheet collapse	2	5	7	0	2	16
Stack topple	0	7	4	3	0	14
Waterline event	25	37	38	33	9	142
Subaqueous event	2	4	4	0	0	10
Unknown	2	1	0	17	0	21
Total	62	84	85	86	41	358
Calving spatial frequency	0.09	0.17	0.09	0.22	0.09	–
Calving-velocity ratio	139.64	111.41	100.83	216.08	362.83	–

collapsing ice (i.e. subaerial or subaqueous), the source of failure in the ice column, and the amount of rotation in the falling section. Calving events were subsequently grouped into five classes: waterline event, ice-fall event, sheet collapse, stack topple, and subaqueous events (Table 1). These characterisations are based on those outlined in previous studies (e.g., Benn and others, 2007; O'Neel and others, 2007; Bartholomaus and others, 2012; Chapuis and Tetzlaff, 2014; Benn and others, 2017; Minowa and others, 2018). The compiled video of the time-lapse imagery and the list of recorded calving events are included as supplementary material in this study.

Location of calving events

The calving front was divided into five sections based on key terminus conditions: 1) the west margin, which is closest to the camera and 660 m wide (determined from the satellite image shown in Fig. 1A); 2) the first plume embayment (named Plume 1), which is 510 m wide; 3) the central headland area, which is 900 m wide; 4) the second plume embayment (named Plume 2), which is 390 m wide; and 5) the east margin, which is furthest away from the camera and 470 m wide (Fig. 1B). The location of each calving event was distinguished manually in the image plane and affiliated with one of these regions.

In addition, the pixel (uv) locations in the image plane were translated to real-world xyz coordinates using the georectification functions available in PyTrx. PyTrx (short for 'Python Tracking') is an open source

photogrammetry toolbox for obtaining measurements from oblique imagery (How and others, 2018). The PyTrx toolbox predominantly utilises functions from the OpenCV computer vision toolbox (opencv.org), and its georectification tools are based on those available in ImGRAFT (imgraft.glaciology.net) (Messerli and Grinsted, 2015). PyTrx is hosted on GitHub (https://github.com/PennyHow/PyTrx) along with the raw data and processing chains for deriving the xyz coordinates.

Several pieces of information were needed to translate the image plane to three-dimensional space. A digital elevation model (DEM) was acquired from TanDEM-X in 2012, with a 10 m spatial resolution. The camera location was surveyed using a Trimble GeoXR GPS rover, which was linked to an SPS855 base station. Positions were differentially post-processed to obtain a horizontal and vertical positional accuracy of 1.20 m and 1.91 m respectively. Ground control points (GCPs) were created from known xyz locations in the camera field-of-view (e.g. features on the adjacent mountain side). Intrinsic matrices and lens distortion parameters were calculated using the camera calibration functions available in the Matlab Computer Vision System Toolbox. The georectified xyz coordinates have an error estimate of 5%, based on uncertainties in the camera parameters (How and others, 2017).

Surface velocities

Surface velocities across the glacier terminus were derived by feature-tracking a pair of TerraSAR-X Synthetic Aperture Radar (SAR) images, at 2 m spatial resolution, collected on the 31st July and 11th August 2015. Feature tracking was applied to the image pair using a 200×200 pixel correlation window (400×400 m), with an uncertainty estimate of <0.4 m per day (as in Luckman and others, 2015). Averages for each region are calculated from these surface velocities, which are used in subsequent analysis.

Velocities could not be determined photogrammetrically from the time-lapse images given that: 1) the glacier is relatively slow-flowing compared to other tidewater outlets in Svalbard; 2) the monitoring period is short which makes it difficult to distinguish small displacements at the glacier surface; and 3) it was difficult to derive velocities with low errors due to the oblique angle of the camera to glacier flow. These factors affected the signal-to-noise ratio in photogrammetric processing, which meant that precise velocity measurements could not be calculated. Therefore, satellite-derived glacier surface velocities were the most robust option for this monitoring period.

CTD measurements

CTD (Conductivity, Temperature, and Depth) water measurements were collected in front of the glacier terminus on the 10th, 13th and 14th August. Specifically, temperature and conductivity readings (from

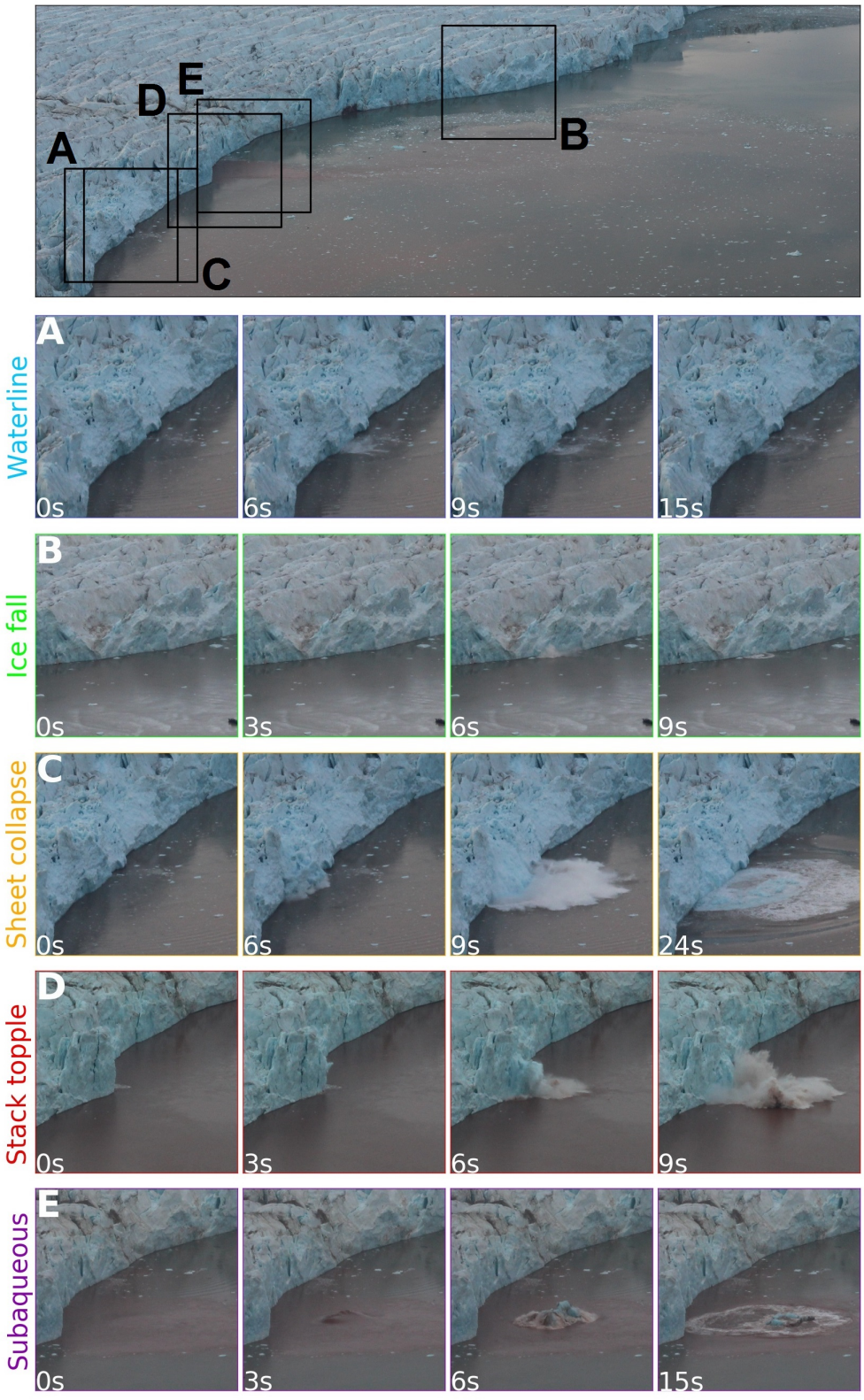

Fig. 2. Picture breakdown of calving styles observed at Tunabreen from 7th–8th August 2015. The top image shows the full calving front with colour-coded extents illustrating where subsequent calving events are located; A) A waterline calving event; B) An ice-fall calving event occurring from the top of the ice column; C) A sheet collapse event where failure at the waterline causes the collapse of a large block of overhead ice; D) A stack topple event where crevasse propagation causes a column of ice to rotate outwards from the terminus and collapse; E) A subaqueous calving event where ice detaches from the ice column below the waterline and upwells to the fjord surface.

which salinity measurements were derived) were collected at the fjord surface and at depths of 2.5 m, 5 m, 7.5 m, 10 m, and 12.5 m below sea level (b.s.l.) (Schild, 2017). All of these measurements (including the location of each spot measurement) are included as supplementary material. Mean values were calculated from these to provide a general overview of the fjord conditions at the time of this study.

Bathymetric data

The seafloor and ice front morphology were mapped using the Kongsberg EM2040 multibeam echosounder, which was mounted on the 15 m research vessel 'Viking Explorer'. These surveys were undertaken on 3rd–5th August, and the 14th August 2015. The survey collected on the 14th August is presented subsequently because it has the best coverage of all the datasets.

The echosounder has a 0.4×0.7 degrees wide beam configuration and the slow survey speeds at the ice front resulted in very high sounding density (hundreds of datapoints per square metre). This allowed generation of digital elevation grids with up to 1 m isometric cell size. Data were processed and visualized using the QPS Fledermaus and GlobalMapper software packages.

Additional oceanic and atmospheric measurements

Tidal level data was obtained from the Norwegian Mapping Authority Hydrographic Service, with measurements recorded every ten minutes (kartverket.no). The tidal level was observed at Ny Ålesund, and adjusted for location (by a multiplication factor of 1.13) and time (minus 17 minutes) to represent water levels in Tempelfjorden. These correction are according to the tidal model used by the Norwegian Mapping Authority Hydrographic Service.

Air temperature measurements were obtained from the weather station situated in Adventdalen, which is managed by the University Centre in Svalbard (https://www.unis.no/resources/weather-stations/). The original data were recorded at one second intervals, but for clarity we present ten-minute averages. Although the Adventdalen weather station is located ∼40 km WSW of Tunabreen, it provides a good estimation of the daily temperature cycle under the prevailing synoptic conditions.

RESULTS

Calving style

Five styles of calving were observed within the 28-hour monitoring period: waterline events, ice-fall events, sheet collapses, stack topples, and subaqueous events (Table 1). The calving front was visible over the course of the entire monitoring period due to the midnight sun and optimal weather conditions, and in

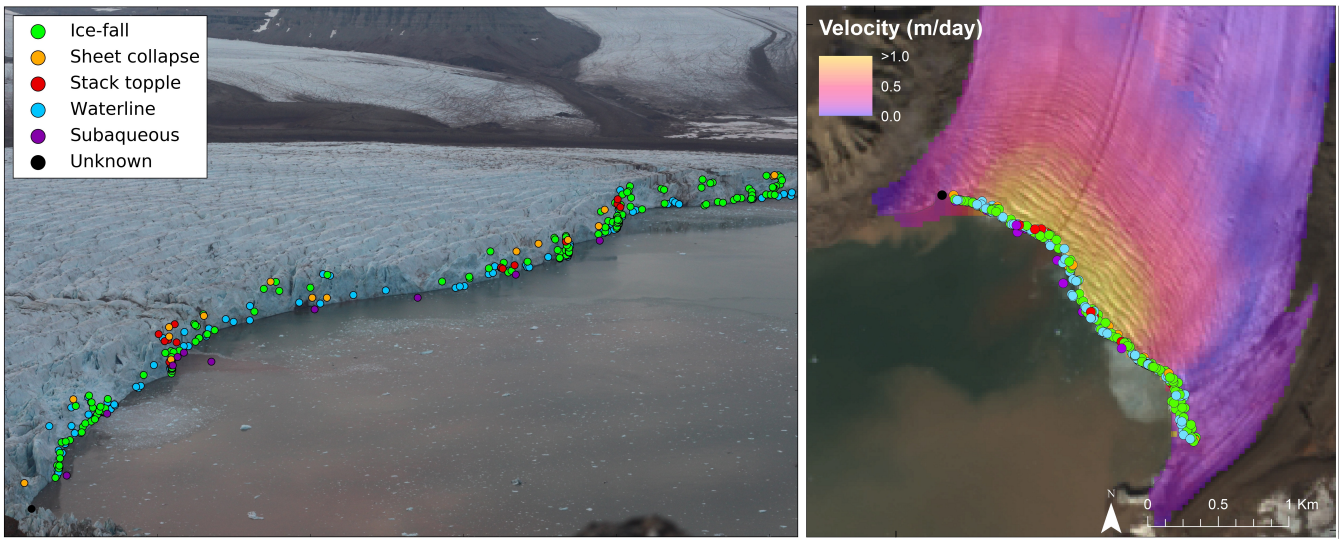

Fig. 3. Calving events observed in the image plane (A) and georectified (B), with the colour of the point denoting the style of calving. Events were manually detected, from which the style of calving was interpreted. The time-lapse image was captured on the 8th August 04:36, and the satellite image is a pan-sharpened Landsat image taken on the 17th August 2015.

---

202 total, 358 calving events were recorded. Waterline and ice-fall events were typically the smallest, whilst
203 sheet and stack topples were the largest (Table 1). These four types of calving events occurred in the
204 subaerial section of the ice front, above the waterline. Subaqueous calving styles involved the break-off of
205 ice from beneath the waterline, producing large, dirty icebergs.

206 Waterline events occurred at, or just above, the waterline (Fig. 2A), resulting in undercutting at the
207 base of the subaerial part of the ice column. Often these events were very small, producing little splash.
208 It is likely that this style of calving event would be undetected by remote seismic monitoring (e.g., Köhler
209 and others, 2015; How, 2018), requiring multiple seismic installations at the glacier terminus in order to
210 increase the chance of detection (e.g., Bartholomaus and others, 2015).

211 Ice-fall events are typified as the break-off of small/medium chunks of ice across the subaerial part of the
212 ice front (Fig. 2B). These occurred at all heights in the ice column, with the break-off of ice from the top
213 of the ice column being easiest to detect because they produced the largest splash. Ice-falls were observed
214 to collapse as a whole body of ice, or disintegrate before they hit the fjord water (Fig. 2B).

215 Sheet collapses consist of large detachments of ice from the terminus (Fig. 2C), where the body of ice
216 collapses downwards with little rotation, hence it looks like a sheet as it enters the fjord water. This can

often affect a sizeable portion of the glacier front where melt-undercutting and/or turbulence generated by wave action is apparent (O'Leary and Christoffersen, 2013; Pętlicki and others, 2015).

Stack topples are another large calving style observed at Tunabreen (Fig. 2D). Failure in the ice column originates from above the waterline, causing large tabular columns of ice to collapse into the fjord water. Rotation in the falling section of ice was observed, rotating out from the glacier front and often exploding on impact and generating ice ballistics that were scattered across the fjord.

Subaqueous calving events occurred below the waterline (Fig. 2E). Although iceberg detachment from the glacier could not be directly observed from the time-lapse camera imagery, we could identify subaqueous calving events from the sudden emergence of icebergs in front of the glacier. Subaqueous events were the least common style of calving, but often produced large icebergs that were heavily freighted with debris. These bergs typically have a dark or deep blue appearance, due to smooth surfaces associated with submarine melt (in contrast, subaerial ice surfaces are typically rough and appear white). Observations of debris-rich ice exposed in stranded bergs and ice cliffs during the winter months show abundant evidence of basal transport and shear (Lovell and others, 2015); and we conclude that the debris-rich ice observed in subaqueously calved bergs originated at, or close to, the base of the glacier similar to those described by Wagner and others (2014).

The majority of calving events (82%) were ice-fall and waterline events, with 155 ice-fall events and 142 waterline events recorded over the monitoring period (Table 2). Sheet collapses and stack topples comprised a smaller proportion of the recorded calving activity, with only 16 sheet collapses and 14 stack topples recorded. Also, only 10 subaqueous events occurred, but these often produced large icebergs that upwelled into the fjord. Of the 358 detected calving events, 21 events could not be confidently classified from the time-lapse sequence. This was either due to poor visibility at the waterline (due to glare of the fjord surface) or partial concealment as a result of the time-lapse camera field of view.

Location of calving events

Calving events occurred across the entire glacier front (Fig. 3), but were abundant in the central region of the terminus, with 84 observed events at Plume 1, 85 observed events in the headland area, and 86 observed events at Plume 2 (Table 2). Fewer events were observed at the margins, with 62 observed events at the west margin (i.e. closest to the camera), and 41 events at the east margin (i.e. furthest away from the camera) (Fig. 1). The normalised values – calving spatial frequency and calving-velocity ratio (Table 2) – were determined using the width of each region of the terminus (as shown in Figure 1B) and its average

surface velocity, respectively. This shows that whilst there was consistent calving activity at the headland and margin regions (0.09 calving events per metre), there was focused calving activity in the plume regions; with 0.17 calving events per metre at Plume 1 and 0.22 calving events per metre at Plume 2. In addition, there is a disproportionate amount of calving at the margins despite slow surface velocities, which indicates that changes in velocity across the terminus are not linked to the total number of calving events observed.

Ice-fall events were the dominant style of calving at the margins of the terminus, with 31 recorded events at the west margin and 30 at the east margin (Table 2). Abundant waterline events were also observed at the west margin, with 25 recorded events (Table 2). Waterline events were the dominant calving style in the central regions of the terminus (Plume 1, Headland, and Plume 2 in Table 2). Ice-fall events were also frequent in these regions. The highest number of sheet collapses was observed at Plume 1 and the headland regions, with 5 recorded sheet collapses at Plume 1 and 7 recorded sheet collapses in the headland region (Table 2). Stack topples occurred only in these two regions also (7 events occurring at Plume 1 and 4 events occurring in the headland region, Table 2). Subaqueous events were observed in the areas nearest to the time-lapse camera (i.e. the west margin, Plume 1, and headland regions in Table 2), however this could merely reflect the difficulty in detecting this style of calving with distance from the camera.

Surface velocities (derived from TerraSAR-X imagery) ranged from 0 to $\sim$1 md^{-1} across the glacier terminus during the monitoring period (Fig. 3B). The fastest flowing part of the terminus is around the glacier centreline, encompassing the two plumes and the headland region (defined in Fig. 1B). These regions experienced the most calving events. In addition, stack topples occurred in Plume 1 and the headland region, which are within the area of fastest flow.

Temporal distribution of calving events

The calving events are not randomly distributed in time, but show clear temporal patterns that allow environmental triggers to be identified. Air temperature measured at the Adventdalen weather station underwent small fluctuations during the observation period, ranging between 6.0°C and 9.1°C and peaking around 16:00 (local time) on the 8th August (Fig. 4). This is typical of stable, clear-sky conditions during the Svalbard summer, when the sun is continuously above the horizon. Tidal levels fluctuated between 0.4 m and 1.5 m, with a tidal range of 1.1 m. The observation period spans a little more than two tidal cycles.

Enhanced calving activity is evident between 08:00 and 14:00 on the 8th August, coinciding with the falling limb (i.e. high-to-low) of the tidal cycle, with 111 events recorded in comparison to 29 events recorded on the prior rising limb (02:00–08:00, 8th August). Of the two full tidal cycles observed during

Table 3. Average CTD measurements taken in front of Tunabreen on the 10th, 13th and 14th August 2015.

Depth	Temperature (°C)*	Conductivity (μS/cm)†	Salinity (psu)‡
Surface	3.52	17993	18.64
2.5 m	3.76	29344	30.62
5.0 m	4.03	30410	31.63
7.5 m	4.40	31312	32.38
10.0 m	4.55	31730	32.73
12.5 m	4.57	31814	32.79

*Temperature readings have an error estimate of ±0.2°C

†Conductivity measurements have an error estimate of ±2.0%

‡Salinity measurements have an error estimate of ±1.0%

this monitoring period (from 19:40, 7th August to 20:30, 8th August), 68% of calving activity (204 events) occurred on the falling limbs of the tide and 32% (96 events) occurred on the rising limbs.

CTD measurements

CTD measurements taken in the fjord close to the glacier front showed that warm, saline water was present below depths of 7.5 m b.s.l., with a mean temperature and salinity of ∼4.5°C and ∼32.6 psu, respectively (Table 3). The water at the surface is cooler (3.5°C) and fresher (18.9 psu) likely due to meltwater runoff and/or floating bergs (Table 3). Temperature and salinity at intermediate depths shows varying degrees of mixing between the surface water and deeper layers.

Bathymetric surveys

The bathymetric mapping of the sea floor covers an area of ∼2 km^2 across the majority of the fjord width (Fig. 5A). The east region of the fjord became very shallow (<10 m b.s.l.) hence why no data could be collected from the fjord water adjacent to the east margin of the glacier. The sea bed topography ranged between 10 m and 70 m b.s.l., with relatively shallow topography present at the boundaries of the survey area. An overdeepening is evident on the west side of the fjord, where topography was between 50 m and 70 m b.s.l.. This overdeepening is adjacent to the exit of one of the meltwater plumes from Tunabreen (with the glacier embayment area surrounding it referred to as Plume 1).

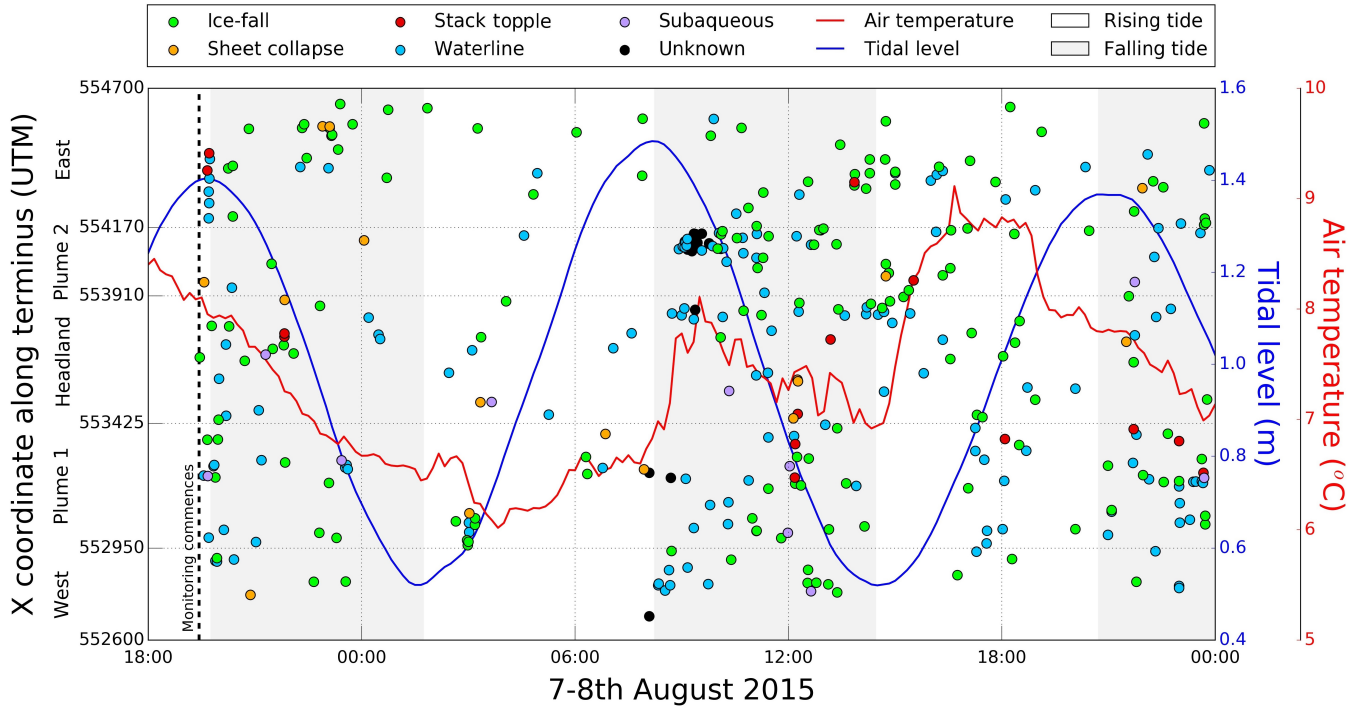

Fig. 4. Space-time plot of the observed calving events, tidal level, and average air temperature. The colour of the point denotes the style of calving. The white and grey shaded regions represent the rising and falling tidal limb, respectively.

The echosounder was tilted in order to survey the submarine part of Tunabreen's calving front in addition to the sea bed survey. A transect of this is presented in Fig. 5B, which was taken in the Plume 1 region of the terminus (see white line in Fig. 5A for transect location). The transect in Fig. 5B depicts all of the soundings along the profile as point measurements. The transect shows a ∼5 m undercut near the glacier bed. This undercut spans 35 m of the vertical submarine ice cliff (from a depth of 25 m to 60 m b.s.l. in Fig. 5B). Above this undercut is a near-vertical ice cliff, which is present from a depth of 25 m b.s.l. to the end of the transect (at a depth of 10 m b.s.l.). This transect shows that there is substantial undercutting of the submarine ice cliff, which is likely to be linked to the presence of a meltwater plume (Fried and others, 2015). In comparing the detected calving events, we find stack topples, sheet collapses and subaqueous events commonly occur in areas where the ice margin is severely undercut, whereas waterline and small ice fall events are common to the entire ice face (Fig. 5A).

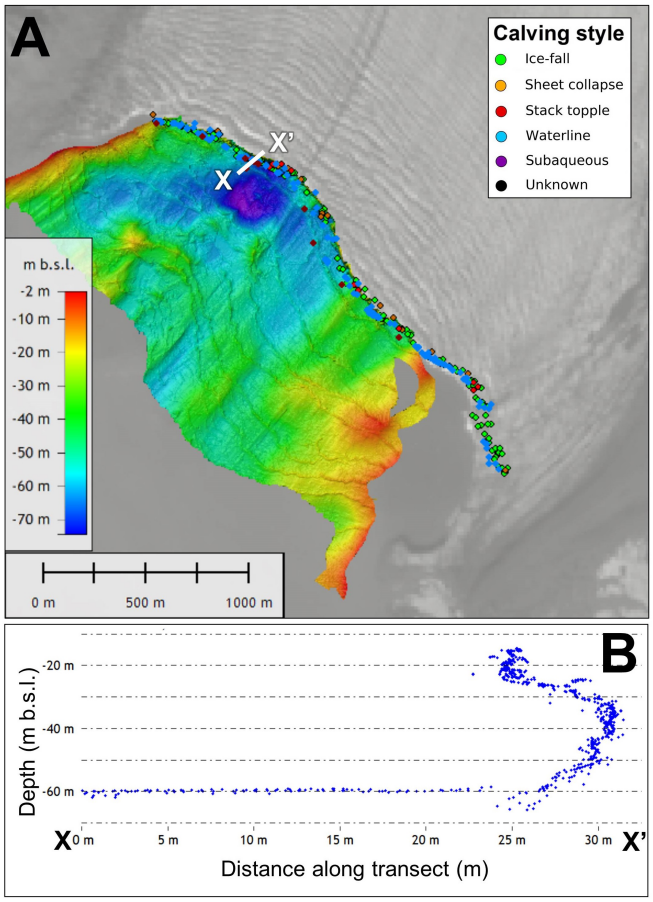

Fig. 5. Bathymetric surveying undertaken in Tempelfjorden on the 14th August 2015. A shows sea bed topography (metres b.s.l.), which covers the majority of the area adjacent to the glacier terminus. Calving events detected with the time-lapse sequence are denoted by the point locations at the terminus, which are colour-coded to calving style (consist with the colour scheme presented in previous figures). The white line signifies the transect of the submarine part of the terminus, which is presented in B. The transect consists of all soundings in a 20 cm wide corridor along the profile.

DISCUSSION

Calving mechanisms at Tunabreen

Five styles of calving have been distinguished: waterline events, ice-fall events, sheet collapses, stack topples, and subaqueous events (Fig. 2). Waterline calving (Fig. 2A) and ice-fall calving (Fig. 2B) are the most common type of event. Waterline and ice-fall events occur across the entire calving front of the glacier, indicating that the mechanism related to these styles of calving are uniform across the terminus.

As previously stated, sheet collapses appear to involve the detachment and downward movement of ice bodies with little rotation (Fig. 2C). These are suggested to be caused by undercutting at the waterline, which is also referred to as 'waterline notching' by Pętlicki and others (2015) who observed similar behaviour at Hansbreen in Svalbard. Stack topples involve the detachment of ice that rotates outwards from the terminus (Fig. 2D). These occur in the central region of the terminus (Table 2) where the glacier flows fastest and thus the ice surface is traversed by numerous transverse crevasses (Fig. 3B), and where the sea bed is deepest (Fig. 5A). This style of calving may therefore be associated with longitudinal stretching of the glacier front and change in buoyancy forcing at the terminus.

Subaqueous calving events (Fig. 2E) are rare, accounting for only 10 of the observed 358 observed events (3%, despite the fact that 60–70% of the terminus is below sea level. Subaqueous calving occurs when buoyant forces acting on a projecting mass of ice (an 'ice foot') exceed the tensile strength of the ice (or the fracture toughness if a pre-existing crack is present), allowing the ice to break free and shoot to the surface (Wagner and others, 2016; Benn and others, 2017; Slater and others, 2017b). Ice feet are formed either by retreat of the subaerial part of the terminus or melting in the upper part of the water column. The extreme rarity of subaqueous calving events compared with subaerial calving indicates that ice foot development is not associated with subaerial cliff retreat at Tunabreen. Rather, submarine melting likely accounts for most ice loss below the waterline, which both isolates projecting ice feet near the base of the cliff and undermines the subaerial portion of the front (Motyka and others, 2003).

The main limitation of this study is that the monitoring period is relatively short, and the findings presented may not reflect all tidewater termini. However, similar observations have been made at other tidewarer glaciers which indicate that the findings at Tunabreen are valid. As previously outlined, subaqueous events make up 3% of the calving activity observed at Tunabreen even though 60–70% of the terminus is below sea level. This is strikingly alike to Yahtse Glacier, where 6% of calving activity is subaqueous and ∼65% of the terminus is below sea level (Bartholomaus and others, 2012). These similarities prevail despite the fact that surface velocities are much faster at Yahtse Glacier (17 md^{-1}) and subsurface ocean temperatures are 3°C warmer than those recorded at the front of Tunabreen on average (Bartholomaus and others, 2013).

Calving event size and frequency

Of the 358 calving events that were observed within the 28-hour time-lapse sequence, 297 events (82%) involved smaller styles of calving (i.e. waterline and ice-fall events) and only 61 were larger styles (i.e. sheet

collapses, stack topples, and subaqueous events). The size-frequency distribution of calving at Tunabreen follows a power law relation (Åström and others, 2014; Vallot and others, 2018b), similar to those observed at other Svalbard glaciers (Chapuis and Tetzlaff, 2014). In these cases, the observed calving frequency distribution is associated with the mutual interplay between calving and instabilities in the local vicinity of the calving region (Schild and others, 2018).

Calving events are preceeded by others in some instances at Tunabreen, such as the consecutive events observed on the second falling tidal limb in Fig. 4 (08:00–14:00, 8th August). This demonstrates that, on occasion, calving events in one region can trigger a chain of enhanced calving activity in adjacent areas (Chapuis and Tetzlaff, 2014). Bartholomaus and others (2012) observed similar instances at Yahtse Glacier in Alaska, noting multiple events over short periods of time (∼10 minutes). This suggests that the calving events within these instances are linked, and reflect periods of instability at discrete regions of the glacier front.'

Calving glacier fronts behave like self-organised critical systems, delicately poised between sub-critical, critical, and super-critical states (Åström and others, 2014). Our data suggests that small styles of calving (i.e. waterline and ice-fall events) play a crucial role in these transitions, as they comprise a high majority of calving activity at Tunabreen (Table 2). Under-representation of small-scale calving events is an inherent problem with many commonly used monitored methods, such as satellite image analysis (e.g., Seale and others, 2011; Schild and Hamilton, 2013), low-temporal-frequency time-lapse photography (e.g., Pętlicki and others, 2015), and seismic event detection from remote stations (e.g., Köhler and others, 2015). High spatio-temporal resolution observations, such as those reported here and previously with both time-lapse and local seismic monitoring (e.g., Bartholomaus and others, 2015; Medrzycka and others, 2016), are crucial in developing a detailed process-based understanding of calving mechanisms.

Critical system behaviour is also evident in the temporal distribution of calving events. Over the two full tidal cycles observed in our record, 68% of the events occurred on the falling limb phases (Fig. 4). This is particularly notable during the falling tidal limb between 08:00 and 14:00 (8th August). A tendency for calving events to cluster on falling and low tides has been noted in previous studies, such as Bartholomaus and others (2015) who found a statistical association between seismically detected calving events and tidal frequencies. This is likely to reflect modulation of the normal stress acting on the glacier terminus. The tidal range in Tempelfjorden is small (1.1 m), representing ∼2% of the back-pressure exerted on the terminus by the water column. Nevertheless, this small reduction in support at the ice front was apparently sufficient

to trigger cascades of calving events. This is symptomatic of a critical system that is sensitive to small perturbations.

The role of melt-undercutting

Waterline and ice-fall calving styles occur across all regions, which is indicative of consistent controls on calving across the terminus. These styles have been observed in the time-lapse imagery to create notches at the waterline, which develop weaknesses in the ice cliff. Similar observations have been made at other glaciers in Svalbard (e.g., Pętlicki and others, 2015), Greenland (e.g., Medrzycka and others, 2016) and Alaska (e.g., Bartholomaus and others, 2012) where weaknesses generated at the waterline cause terminus instability, resulting in the short-term excavation of ice through small, frequent calving events.

The high concentration of calving events and different calving styles at Plume 1 and Plume 2 is consistent with the idea that enhanced undercutting takes place at the locations of meltwater plumes (Fig. 3A and Fig. 4). CTD measurements (Table 3) show that cold, fresh meltwater entering the fjord at depth would encounter warm, saline fjord water, encouraging rapid buoyant ascent. This would lead to efficient water mixing and high melt rates in the vicinity of the plumes (Jenkins, 2011; Slater and others, 2017b; Vallot and others, 2018a). The presence of an undercut is further supported by observations from the bathymetric surveys in this study, revealing the presence of extensive undercutting below the waterline at Plume 1 (Fig. 5).

It is also possible that calving events themselves act as another contributor to turbulence at the waterline. The waves generated by large calving events and high-falling icebergs will likely bring warm water into contact with the front and also dislodge sections of ice at the waterline. This is likely an additional contributing factor to the occurrence of multiple calving events over short periods of time (Fig. 4), indicating that ice is episodically removed rather than gradually over the course of the melt season. Similar instances of the episodic ice loss have also been observed at other tidewater glaciers in Svalbard (e.g., Chapuis and Tetzlaff, 2014) and Alaska (e.g. Bartholomaus and others, 2012).

The calving styles reported here bear a strong resemblance to 'low-magnitude' calving events in HiDEM simulations reported by Benn and others (2017). That is, they are localised collapses of the subaerial ice cliff following loss of support from beneath. However, our record does not contain any events resembling the 'high-magnitude' events described by Benn and others (2017). This is likely to be attributed to Tunabreen's grounded terminus and inability to form significant undercuts, which limits the size of calving bergs. Model results showed that 'low-magnitude' events simply remove part of the unsupported overhang, and this is

possibly the case at Tunabreen – small, frequent calving activity limit the formation of large undercuts. The observed calving styles at Tunabreen for this observation period therefore suggest that calving may simply follow the pace set by submarine melting, and do not amplify rates of frontal ablation. In such cases, models of calving rate may be formulated by simply calculating the rate of submarine melting (Luckman and others, 2015). This possibility will be tested in future work. Automated methods to detect and classify calving events are needed in order to assist in this endeavour, such as from time-lapse imagery (e.g., Vallot and others, 2018b), video (e.g., Bartholomaus and others, 2012), and seismic records (e.g., O'Neel and others, 2007; Köhler and others, 2015; Mei and others, 2017).

CONCLUSIONS

In this study, we documented calving events at Tunabreen using a high-frequency time-lapse sequence covering a 28-hour period in August 2015. The sequence consists of 34,117 images, which has enabled examination of the individual calving styles active at Tunabreen, and identification of the key controls and triggers of calving events. Despite the short data record, our observations are consistent with previous findings at Tunabreen (Åström and others, 2014; Köhler and others, 2015; Vallot and others, 2018b) and allow the mechanisms of failure to be examined in greater detail than hitherto possible.

Calving activity at Tunabreen is characterised by frequent events (12.8 events per hour), with 358 distinguished events in the 28-hour monitoring period. Calving events were partitioned into five categories based upon relative size and failure mechanism: waterline events, ice-fall events, sheet collapses, stack topples, and subaqueous events. Waterline and ice-fall events make up a high proportion of all calving events (82%), which consist of small occurrences that originated at, or a small distance above, the waterline. The two larger subaerial styles (sheet collapses and stack topples) differ in the observed rotation of the ice body as it hits the water. Ice bodies undergoes little rotation with sheet collapses, whereas ice bodies rotate outwards from the terminus with stack topples. As stack topples are largely confined to the fastest flowing region of the terminus where the sea bed is deepest (primarily the Headland region), this suggests that controls on calving vary across the terminus and, in this case, these changes are primarily associated with longitudinal stretching and water depth. The majority of events (97%) originated from the subaerial section of the ice cliff, despite the fact that 60–70% of the terminus is below sea level. The rarity of subaqueous events indicates that ice loss below the waterline is dominated by submarine melting, with only local development of projecting 'ice feet'.

Weighted by the width of the ice front, calving events are roughly twice as frequent in the vicinity of meltwater plumes compared to non-plume areas. In these areas, the ascent of buoyant meltwater and entrainment of warm, saline fjord water encourages more rapid subaqueous melting and undercutting of the subaerial ice cliff. This is supported by the bathymetric surveys of the submarine part of the terminus, which show a ∼5 m undercut at the base of the glacier.

Across the terminus width, a large proportion (68%) of calving events occurred on the falling limb of the tidal cycle. The tidal range represents only ∼2% of the backstress exerted on the terminus by the water column, suggesting that terminus stability is highly sensitive to tidal variation. Taken together, the observations support the conclusion that the terminus is a critical system, responsive to small changes in environmental conditions (Åström and others, 2014; Chapuis and Tetzlaff, 2014; Bartholomaus and others, 2015).

Multiple calving events were observed to occur over short periods. These typically consist of numerous small events, which have been observed by others to promote larger collapses and may suggest that small-scale calving events play a crucial role in terminus stability (Bartholomaus and others, 2012; Medrzycka and others, 2016). In addition, the occurrence of multiple calving events suggests that ice is episodically removed from the terminus rather than gradually over time. Similar observations have been made at other tidewater glaciers in Svalbard (e.g., Pętlicki and others, 2015), Alaska (e.g., Motyka and others, 2003; Bartholomaus and others, 2012), and have been simulated in models such as the particle model, HiDEM (Benn and others, 2017). Beyond this study, it is unknown how undercutting and calving processes change throughout a melt season at Tunabreen, but it is expected that meltwater availability and fjord temperatures would play crucial roles in this (Luckman and others, 2015; Slater and others, 2017b).

The calving styles reported here strongly resemble those simulated by the HiDEM particle model (Benn and others, 2017), which suggests that calving rates at Tunabreen for this observation period may simply be paced by the rate of submarine melting. Similar dynamics have also been observed at other tidewater glaciers in Svalbard (e.g., Chapuis and Tetzlaff, 2014; Pętlicki and others, 2015), Greenland (e.g., Medrzycka and others, 2016) and Alaska (e.g., Bartholomaus and others, 2012, 2015) which further strengthen this idea. The inference of calving rate from submarine melt rate would greatly simplify the challenge of incorporating the effect of melt-undercutting in predictive numerical models; at least for this type of well-grounded, highly fractured glacier. Detailed observations of small-scale calving mechanisms at high temporal frequency may

458 therefore help us develop the theoretical understanding necessary for the development of models that
459 faithfully reflect the realities of frontal ablation.

460 SUPPLEMENTARY MATERIAL

461 The supplementary material to this study comprises of the time-lapse video sequence (1), a record of all
462 defined calving events (2), and the CTD fjord measurements (3).

463 CONTRIBUTION STATEMENT

464 PH is the primary author of this paper and was responsible for the time-lapse camera installations
465 and subsequent imagery processing and analysis. KMS collected the CTD measurements and assisted
466 in developing the ideas presented. DIB is the project leader, co-ordinated the field work, and assisted in
467 developing the ideas presented. RN and NK were responsible for the bathymetry surveys and analysis. AL
468 provided glacier velocities and the TanDEM-X DEM data. DV assisted in the field and advised on the
469 time-lapse analysis. NRJH assisted in the development of the time-lapse camera systems. CB assisted in
470 the field and advised on the development of this paper.

471 ACKNOWLEDGEMENTS

472 This work is affiliated with the CRIOS project (Calving Rates and Impact On Sea Level), which was
473 supported by the Conoco Phillips-Lundin Northern Area Program. PH is funded by a NERC PhD
474 studentship (reference number 1396698). The TanDEM-X DEM data were kindly provided by DLR through
475 the Intermediate DEM opportunity (project IDEM_GLAC0213), and TerraSAR-X data were provided by
476 DLR project number OCE1503. The fieldwork associated with this work would not have been possible
477 without the logistical support provided by the University Centre in Svalbard Tech and Logistics team. We
478 greatly acknowledge Alex Hart and the GeoSciences Mechanical Workshop at the University of Edinburgh
479 for manufacturing the time-lapse camera enclosure that was used in this study. We would also like to thank
480 Jack Kohler and Airlift AS for offering an opportunistic flight over the field site, and Anne Flink, Oscar
481 Fransner, and Richard Delf for their assistance in the field. And finally many thanks to the scientific editor,
482 Dr. Toby Meierbachtol, and Dr. Timothy Bartholomaus and one anonymous reviewer for their insightful
483 and constructive feedback on this manuscript.

REFERENCES

Åström JA and 10 others (2014) Termini of calving glaciers as self-organized critical systems. *Nat. Geosci.*, **7**(12), 874–878, (doi: 10.1038/ngeo2290)

Bartholomaus TC, Larsen CF, O'Neel S and West ME (2012) Calving seismicity from iceberg-sea surface interactions. *J. Geophys. Res.*, **117**, F04029, (doi: 10.1029/2012JF002513)

Bartholomaus TC, Larsen CF and O'Neel S (2013) Does calving matter? Evidence for significant submarine melt. *Earth Planet. Sci. Lett.*, **380**, 21–30, (doi: 10.1016/j.epsl.2013.08.014)

Bartholomaus TC, Larsen CF, West ME, O'Neel S, Pettit EC and Truffer M (2015) Tidal and seasonal variations in calving flux observed with passive seismology. *J. Geophys. Res. Earth Surf.*, **120**(11), 2318-2337, (doi: 10.1002/2015JF003641)

Benn DI, Warren CR and Mottram RH (2007) Calving processes and the dynamics of calving glaciers. *Earth. Sci. Rev.*, **82**(3), 143–179, (doi: 10.1016/j.earscirev.2007.02.002)

Benn DI and 7 others (2017) Melt-under-cutting and buoyancy-driven calving from tidewater glaciers: new insights from discrete element and continuum model simulations. *J. Glaciol.*, **63**(240), 691–702, (doi: 10.1017/jog.2017.41)

Chapuis A and Tetzlaff T (2014) The variability of tidewater-glacier calving: Origin of event-size and interval distributions. *J. Glaciol.*, **60**(222), 622–634, (doi: 10.3189/2014JoG13J215)

Chauché N and 8 others (2014) Ice-ocean interaction and calving front morphology at two west Greenland tidewater outlet glaciers. *Cryosphere*, **8**(4), 1457–1468, (doi: 10.5194/tc-8-1457-2014)

Cottier F, Tverberg V, Inall M, Svendsen H, Nilsen F and Griffiths C (2005) Water mass modification in an Arctic fjord through cross-shelf exchange: The seasonal hydrography of Kongsfjorden, Svalbard. *J. Geophys. Res.-Oceans*, **110**, C12005, (doi: 10.1029/2004JC002757)

Cowton T, Slater D, Sole A, Goldberg D and Nienow P (2015) Modeling the impact of glacial runoff on fjord circulation and submarine melt rate using a new subgrid-scale parameterization for glacial plumes. *J. Geophy. Res.-Oceans*, **120**(2), 796–812, (doi: 10.1002/2014JC010324)

Flink AE, Noormets R, Kirchner N, Benn DI, Luckman A and Lovell H (2015) The evolution of a submarine landform record following recent and multiple surges of Tunabreen glacier, Svalbard. *Quat. Sci. Rev.*, **108**, 37–50, (doi: 10.1016/j.quascirev.2014.11.006)

Fried MJ and 8 others (2015) Distributed subglacial discharge drives significant submarine melt at a Greenland tidewater glacier. *Geophys. Res. Lett.*, **42**(21), 9328–9336, (doi: 10.1002/2015GL065806)

Holland DM, Thomas RH, de Young B, Ribergaard MH and Lyberth B (2015) Acceleration of Jakobshavn Isbrætriggered by warm subsurface ocean waters. *Nat. Geosci.*, **1**, 659–664, (doi: 10.1038/ngeo316)

How P (2018) *Dynamical change at tidewater glaciers examined using time-lapse photogrammetry.* PhD thesis, University of Edinburgh, Edinburgh.

How P and 9 others (2017) Rapidly changing subglacial hydrological pathways at a tidewater glacier revealed through simultaneous observations of water pressure, supraglacial lakes, meltwater plumes and surface velocities. *Cryosphere*, **11**(6), 2691–2710 (doi: 10.5194/tc-11-2691-2017)

How P, Hulton NRJ and Buie L (2018) PyTrx: A Python toolbox for deriving velocities, surface areas and line measurements from oblique imagery in glacial environments. *Geosci. Instrum. Method. Data Syst. Discuss.*, in review, (doi: 10.5194/gi-2018-28)

Howat IM, Box JE, Ahn Y, Herrington A and McFadden EM (2010) Seasonal variability in the dynamics of marine-terminating outlet glaciers in Greenland. *J. Glaciol.*, **56**(198), 601–613, (doi: 10.3189/002214310793146232)

James TD, Murray T, Selmes N, Scharrer K and O'Leary M (2015) Buoyant flexure and basal crevassing in dynamic mass loss at Helheim Glacier. *Nat. Geosci.*, **7**(8), 593–596, (doi: 10.1038/ngeo2204)

Jenkins A (2011) Convection-driven melting near the grounding lines of ice shelves and tidewater glaciers. *J. Phys. Oceanogr.*, **41**(12), 2279–2294, (doi: 10.1175/JPO-D-11-03.1)

Joughin I and 8 others (2008) Ice-front variation and tidewater behavior on Helheim and Kangerdlugssuaq Glaciers, Greenland. *J. Geophys. Res.*, **113**(F1), F01004, (doi: 10.1029/2007JF000837)

Köhler A, Nuth C, Schweitzer J, Weidle C and Gibbons SJ (2015) Regional passive seismic monitoring reveals dynamic glacier activity on Spitsbergen, Svalbard. *Polar Res.*, **34**, 26178, (doi: 10.3402/polar.v34.26178)

Lovell H, Fleming EJ, Benn DI, Hubbard B, Lukas S and Naegeli K (2015) Former dynamic behaviour of a cold-based valley glacier on Svalbard revealed by basal ice and structural glaciology investigations. *J. Glaciol.*, **61**(226), 309–328, (doi: 10.3189/2015JoG14J120)

Luckman A, Benn DI, Cottier F, Bevan S, Nilsen F and Inall M (2015) Calving rates at tidewater glaciers vary strongly with ocean temperature. *Nat. Commun.*, **6**, 8566, (doi: 10.1038/ncomms9566)

Medrzycka D, Benn DI, Box JE, Copland L and Balog J (2016) Calving behavior at Rink Isbræ, West Greenland, from time-lapse photos. *Arct. Antarct. Alp. Res.*, **48**(2), 263–277, (doi: 10.1657/AAAR0015-059)

Mei MJ, Holland DM, Anandakrishnan S, and Zheng T (2017) Calving localization at Helheim Glacier using multiple local seismic stations. *Cryosphere*, **11**, 609–618, (doi: 10.5194/tc-11-609-2017)

Messerli A and Grinsted A (2015) Image GeoRectification And Feature Tracking toolbox: ImGRAFT. *Geosci. Instrum. Method. Data Syst.*, **4**(1), 23–34, (doi: 10.5194/gi-4-23-2015)

Minowa M, Podolskiy EA, Sugiyama S, Sakakibara D and Skvarca P (2018) Glacier calving observed with time-lapse imagery and tsunami waves at Glaciar Perito Moreno, Patagonia. *J. Glaciol.*, **64**(245), 362–376, (doi: 10.1017/jog.2018.28)

Motyka RJ, Hunter L, Echelmeyer KA and Connor C (2003) Submarine melting at the terminus of a temperate tidewater glacier, LeConte Glacier, Alaska, U.S.A. *Ann. Glaciol.*, **36**, 57–65, (doi: 10.3189/172756403781816374)

O'Leary M and Christoffersen P (2013) Calving on tidewater glaciers amplified by submarine frontal melting. *Cryosphere*, **7**(1), 119–128, (doi: 10.5194/tc-7-119-2013)

O'Neel S, Marshall HP, McNamara DE and Pfeffer WT (2007) Seismic detection and analysis of icequakes at Columbia Glacier, Alaska, *J. Geophys. Res.*, **112**, F03S23, (doi: 10.1029/2006JF000595)

Pętlicki M, Ciepły M, Jania JA, Promińska A and Kinnard C (2015) Calving of a tidewater glacier driven by melting at the waterline. *J. Glaciol.*, **61**(229), 851–863, (doi: 10.3189/2015JoG15J062)

Rignot E, Fenty I, Xu Y, Cai C and Kemp C (2015) Undercutting of marine-terminating glaciers in West Greenland. *Geophys. Res. Lett.*, **42**(14), 5909–5917, (doi: 10.1002/2015GL064236)

Rosenau R, Schwalbe E, Maas HG, Baessler M and Dietrich R (2013) Grounding line migration and high-resolution calving dynamics of Jakobshavn Isbræ, West Greenland. *J. Geophys. Res. Earth Surf.*, **118**(2), 382–395, (doi: 10.1029/2012JF002515)

Schild KM (2017) *The Influence of Subglacial Hydrology on Arctic Tidewater Glaciers and Fjords.* PhD thesis, Darmouth College, New Hampshire

Schild KM and Hamilton GS (2013) Seasonal variations of outlet glacier terminus position in Greenland. *J. Glaciol.*, **59**(216), 759–770, (doi: 10.3189/2013JoG12J238)

Schild KM, Hawley RL and Morriss BF (2016) Subglacial hydrology at Rink Isbræ, West Greenland inferred from sediment plume appearance. *Ann. Glaciol.*, **57**(72), 118–127, (doi: 10.1017/aog.2016.1)

Schild KM and 9 others (2018) Calving rates due to subglacial discharge, fjord circulation, and free convection. *J. Geophys. Res. Earth Surf.*, (doi: 10.1029/2017JF004520)

Seale A, Christoffersen P, Mugford RI and O'Leary M (2011) Ocean forcing of the Greenland Ice Sheet: Calving fronts and patterns of retreat identified by automatic satellite monitoring of eastern outlet glaciers. *J. Geophys. Res.*, **116**, F03013, (doi: 10.1029/2010F001847)

Slater D, Nienow PW, Cowton TR, Goldberg DN and Sole AJ (2015) Effect of near-terminus subglacial hydrology on tidewater glacier submarine melt rates. *Geophs. Res. Lett.*, **42**(8), 2861–2868, (doi: 10.1002/2014GL062494)

Slater D and 6 others (2017a) Spatially distributed runoff at the grounding line of a large Greeenlandic tidewater glacier inferred from plume modelling. *J. Glaciol.*, **63**(238), 309–323, (doi: 10.1017/jog.2016.13)

Slater D, Nienow PW, Goldberg DN, Cowton TR and Sole AJ (2017b) A model for tidewater glacier undercutting by submarine melting. *Geophys. Res. Lett.*, **44**(5), 2360–2368, (doi: 10.1002/2016GL072374)

Straneo F and 7 others (2010) Rapid circulation of warm subtropical waters in a major glacial fjord in East Greenland. *Nat. Geosci.*, **3**(3), 36–43, (doi: 10.1038/nature12854)

579 Sutherland DA, Roth G, Hamilton GS, Mernild SH, Stearns L and Straneo F (2014) Quantifying flow regimes in a
580 Greenland glacial fjord using iceberg drifters. *Geophys. Res. Lett.*, **41**(23), 8411–8420, (doi: 10.1002/2014GL062256)
581 Truffer M and Motyka RJ (2016) Where glaciers meet water: Subaqueous melt and its relevance to glaciers in various
582 settings. *Reviews of Geophys.*, **54**(1), 220–239, (doi: 10.1002/2015RG000494)
583 Vallot D and 9 others (2018a) Effects of undercutting and sliding on calving: a global approach applied to Kronebreen,
584 Svalbard. *Cryosphere*, **12**(2), 609–625, (doi: 10.5194/tc-12-609-2018)
585 Vallot D and 6 others (2018b) Automatic detection of calving events with a time-lapse camera in Tunabreen, Svalbard.
586 *Geosci. Instrum. Method. Data Syst. Discuss.*, in review, (doi: 10.5194/gi-2018-5)
587 Van Der Veen CJ (2002) Calving glaciers. *Prog. Phys. Geogr.*, **26**(1), 96–122, (doi: 10.1191/0309133302pp327ra)
588 Wagner TJW and 8 others (2014) The 'footloose' mechanism: Iceberg decay from hydrostatic stresses. *Geophys. Res.*
589 *Lett.*, **41**(15), 5522–5529, (doi: 10.1002/2014GL060832)
590 Wagner TJW, James TD, Murray T and Vella D (2016) On the role of buoyant flexure in glacier calving. *Geophys.*
591 *Res. Lett.*, **43**(1), 232–240A, (doi: 10.1002/2015GL067247)
592 Welty EZ, Bartholomaus TC, O'Neel S and Pfeffer WT (2013) Cameras as clocks. *J. Glaciol.*, **59**(214), 275–286,
593 (doi: 10.3189/2013JoG12J126)